

Supporting Information: Evaluating different classes of porous materials for carbon capture

Johanna M. Huck^{1,2}, Li-Chiang Lin¹, Adam H. Berger³, Mahdi Niknam Sharak^{1,4}, Richard L. Martin⁵, Abhoyjit S. Bhowm³, Maciej Haranczyk⁵, Karsten Reuter², and Berend Smit^{1,6,7}

¹*Dept. of Chemical and Biomolecular Engineering, University of California, Berkeley, CA 94720*

²*Chair for Theoretical Chemistry and Catalysis Research Center, Technische Universität München, Garching, Germany*

³*Electric Power Research Institute (EPRI), 3420 Hillview Avenue, Palo Alto, CA 94304*

⁴*Department of Chemical Engineering, Quchan University of Advanced Technologies, Quchan, Iran*

⁵*Computational Research Division, Lawrence Berkeley National Laboratory, Berkeley, CA 94720*

⁶*Materials Sciences Division, Lawrence Berkeley National Laboratory, Berkeley, CA 94720*

⁷*Laboratory of molecular simulation, Institut des Sciences et Ingénierie Chimiques, Ecole Polytechnique Fédérale de Lausanne (EPFL), CH-1015 Lausanne, Switzerland*

1 Ideal adsorbed solution theory versus competitive Langmuir adsorption model

For the concept of parasitic energy it is essential to specify the influence of the used mixture model on the energy requirement estimation. Therefore parasitic energy was calculated for all investigated materials by means of predicted mixture isotherms using Ideal Adsorbed Solution Theory (IAST) and competitive model to detect potential differences. Figure 1 illustrates the parasitic energy results using both mixture isotherm predictions. The results of the competitive model are shown as function of the IAST results in a double logarithmic plot. For the majority of materials both models exhibit almost equal parasitic energies. In particular in the higher parasitic energy region, 1000 kJ/kg CO_2 and higher, the IAST results are in good agreement to these of the competitive model as most materials with the exception of a few are located on or close to the diagonal dashed line. These structures, strictly speaking, the synthesized materials PPN-6, PPN-6-CH₂Cl, PPN-6-SO₃H, PPN-6-SO₃Li and the theoretical materials ZIF-40-GIS and ZIF-116-CAG exhibit a quite large CO₂ selectivity in IAST compared to the results from the competitive approach, causing such high differences.

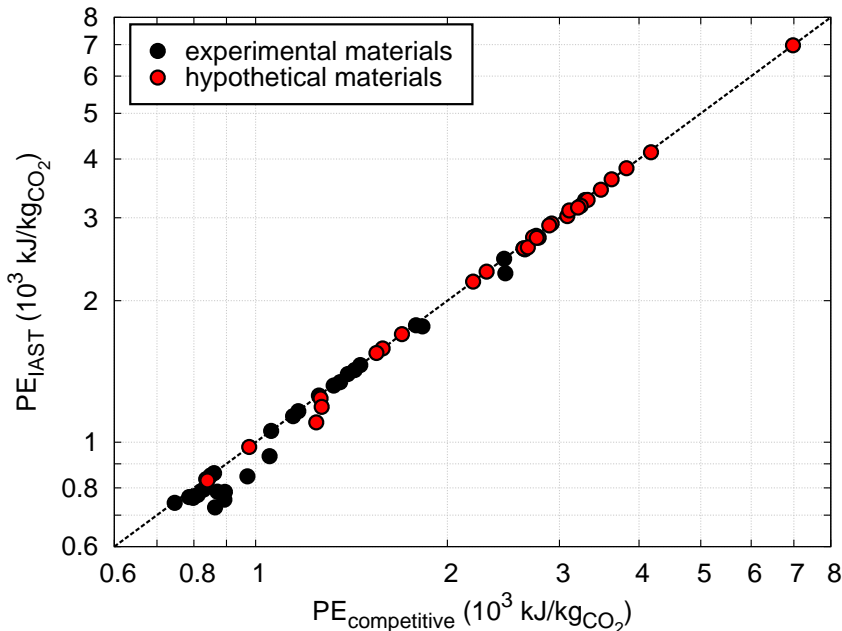


Figure 1: Comparison of IAST and Competitive model based parasitic energies for coal flue gas. Dashed diagonal line illustrates degree of consistency between the results of both models. Results based on experimental data are shown as black circles. Theoretical results are marked as red circles. Mg-MOF-74 exhibits highest parasitic energy difference of $\sim 16\%$ ($\text{PE}_{\text{IAST}} = 727.12 \text{ kJ/kgCO}_2$, $\text{PE}_{\text{comp}} = 863.74 \text{ kJ/kgCO}_2$).

Examining the significant low parasitic energy region (< 1000 kJ/kg CO_2) also reveals intensified aberrations between the results. The parasitic energy results on the basis of IAST tend to predict lower energy requirements than using the competitive model. Materials that are affected particularly are Mg-MOF-74, mmen-CuBTTri, PPN-6-SO₃H, CaA, CaX and NaX. These discrepancies can be explained by the presence of strong binding sites. All affected materials are known to exhibit strong binding sites like open-metal sites (Mg-MOF-74)¹, extraframework cations (CaA, CaX and NaX)² and additional functional groups (mmen-CuBTTri)³. Due to these strong binding sites IAST predicts a higher CO₂ : N₂ selectivity for these materials and thus higher CO₂ purities. Resulting less compression work is needed to reach the intended pressure of 150 bar for transportation and storage. The metal-organic framework Mg-MOF-74 indicates the largest difference of $\sim 16\%$. Investigating simulated mixture isotherms of coal flue gas in Mg-MOF-74 have shown that the predictions of IAST are in a good agreement.¹ Thus, the parasitic energy results used in the main article are based on the IAST approach for the prediction of the mixture isotherms.

2 Calculating the minimal separation work

The basic equation to estimate the minimum energy (W_{sep}^{\min}) required to separate a two-component gas mixture is given by

$$\begin{aligned} -W_{\text{sep}}^{\min} &= T \Delta S \\ &= n_{\text{em}} T s^{\text{im}}(x_{\text{em}}) + n_{\text{cap}} T s^{\text{im}}(x_{\text{cap}}) - n_{\text{flue}} T s^{\text{im}}(x_{\text{flue}}) \end{aligned} \quad (1)$$

where n_{em} is the number of moles of the emitted gas, n_{cap} is the number of moles of the captured gas, and n_{flue} is the number of moles of the flue gas. Similarly, x_{em} corresponds to the mole fraction of emitted CO₂, x_{cap} corresponds to the mole fraction of captured CO₂, and x_{flue} corresponds to the initial mole fraction of CO₂ in the flue gas. Note that all introduced terms are based on the CO₂ concentration of the respective gas. To estimate the correct minimum energy various cases need to be differentiated. Depending on the CO₂ and inert gas composition of the resulting captured and emitted gas stream we need to include or omit different terms in equation (1). In case of complete separation, resulting in pure CO₂ in the captured gas stream and pure inert gas in the emission stream, both particular molar entropies ($s^{\text{im}}(x_{\text{cap}})$ and $s^{\text{im}}(x_{\text{em}})$) do not contribute to the minimum separation energy. The total number of configurations Ω to capture pure CO₂ and emit pure inert gas equals 1, respectively. Accordingly, the contributing entropies $s^{\text{im}}(x_{\text{cap}})$ and $s^{\text{im}}(x_{\text{em}})$ equal 0, due to

$$s^{\text{im}} \propto \ln \Omega \quad (2)$$

Hence, equation (1) reduces to

$$-W_{\text{sep}}^{\min} = -n_{\text{flue}} T s^{\text{im}}(x_{\text{flue}}) \quad (3)$$

On the other hand, if the gas separation is not 100% complete and CO₂ residue is also present in the emitted gas, whereas the captured gas stream contains pure CO₂, only the molar entropy of x_{cap} needs to be omitted. The molar entropy of x_{em} , however, contributes to the minimum energy and changes equation (1) to

$$-W_{\text{sep}}^{\min} = n_{\text{em}} T s^{\text{im}}(x_{\text{em}}) - n_{\text{flue}} T s^{\text{im}}(x_{\text{flue}}) \quad (4)$$

and vice versa to

$$-W_{\text{sep}}^{\min} = n_{\text{cap}} T s^{\text{im}}(x_{\text{cap}}) - n_{\text{flue}} T s^{\text{im}}(x_{\text{flue}}) \quad (5)$$

in case of emitting pure inert gas, while inert gas residue remain in the captured gas stream.

For the remaining entropies in equations (1), (3)-(5) in case of $x \neq 0, 1$ the individual molar entropies of an ideal two-component gas mixture can generally be derived using correlation (2) and the Stirling approximation

$$\ln N! \approx N \ln N - N$$

which results in

$$s^{\text{im}}(x) = R[x \ln x + (1-x) \ln(1-x)] \quad (6)$$

where R is the gas constant and x corresponds to the corresponding mole fraction. Forming the mass balance for the total gas and the CO₂ proportionate gas, results in the following equations:

$$n_{\text{flue}} = n_{\text{cap}} + n_{\text{em}} \quad (7)$$

$$x_{\text{flue}} n_{\text{flue}} = x_{\text{cap}} n_{\text{cap}} + x_{\text{em}} n_{\text{em}} \quad (8)$$

Using equations (7) and (8) one can determine n_{cap} and n_{em}

$$n_{\text{cap}} = \frac{x_{\text{flue}} - x_{\text{em}}}{x_{\text{cap}} - x_{\text{em}}} n_{\text{flue}} \quad (9)$$

$$n_{\text{em}} = \frac{x_{\text{flue}} - x_{\text{cap}}}{x_{\text{em}} - x_{\text{cap}}} n_{\text{flue}} \quad (10)$$

Furthermore, an additional parameter α can be introduced if one aims for a specific CO₂ capture efficiency. In this case the captured and emitted CO₂ fractions can be expressed as the ratio of the initial CO₂ concentration in the flue gas. Consequently, n_{cap} and n_{em} yield in

$$n_{\text{cap}} = \frac{\alpha x_{\text{flue}}}{x_{\text{cap}}} n_{\text{flue}} \quad (11)$$

$$n_{\text{em}} = \frac{(1-\alpha)x_{\text{flue}}}{x_{\text{em}}} n_{\text{flue}} \quad (12)$$

Usually, variable x_{cap} is known for a specific separation process, as it corresponds to the aimed concentration of captured CO₂. However, x_{em} needs to be determined by equalizing equation (10) and (12), which results in

$$x_{\text{em}} = \frac{(1 - \alpha)x_{\text{flue}}x_{\text{cap}}}{x_{\text{cap}} - \alpha x_{\text{flue}}} \quad (13)$$

In the following several minimum separation energies are calculated at different initial gas compositions, CO₂ capture efficiencies, and separation temperatures.

Table 1: Min. separation work (in kJ/kgCO₂) for different initial gas & capture conditions ($n_{\text{flue}} = 1$ mol).

CO ₂ capture efficiency α	W_{sep}^{\min} at 298 K $x_{\text{flue}} = 0.12, x_{\text{cap}} = 1$	W_{sep}^{\min} at 313 K $x_{\text{flue}} = 0.13, x_{\text{cap}} = 1$	W_{sep}^{\min} at 313 K $x_{\text{flue}} = 0.13, x_{\text{cap}} = 0.9$
1	172.2 ⁴	175.8 ⁵	154.4
0.9	158.1 ^{4,6}	161.1 ⁵	139.8

Finally, the value corresponding to parasitic energy can be estimated. In our model of parasitic energy no constant CO₂ capture efficiency is assumed. In an ideal case, however, i.e. the material adsorb all the present CO₂, α equals to 1. The CO₂ mole fraction in the flue gas is set to be $x_{\text{flue}} = 0.14$, $T = 313$ K, and the mole fraction at desorption conditions is 99:1, i.e. $x_{\text{cap}} = 0.99$, and $x_{\text{em}} = 0$ as pure inert gas is emitted. The resulting minimum energy for separation equals $W_{\text{sep}}^{\min} = 167.7$ kJ/kgCO₂. Analogically, the minimum energy for $\alpha = 0.9$ yields in $W_{\text{sep}}^{\min} = 153.1$ kJ/kgCO₂.

3 Envelope lines for coal and natural gas

To specify more reliable envelope lines for the coal and natural gas results, we predicted parasitic energies using the dataset published by Lin et. al.⁷ based on the IAST model for a bi-component mixture gas. The functional form applied to fit the envelope lines was determined to be

$$f(x) = \frac{a}{x^n} + b \cdot x^m \quad (14)$$

To get a reasonable dataset of values which represents the envelope of each gas composition to perform the fitting, we applied the method of bins in x- and y-direction.

Figure 2a and 2b show the parasitic energy results for the coal and natural gas composition, respectively. The red circles illustrate the parasitic energies of the IZA zeolite structures as well as the predicted structures. As dashed lines the fitted envelopes for both flue gases are shown. Furthermore, the fit functions for both envelope lines are included.

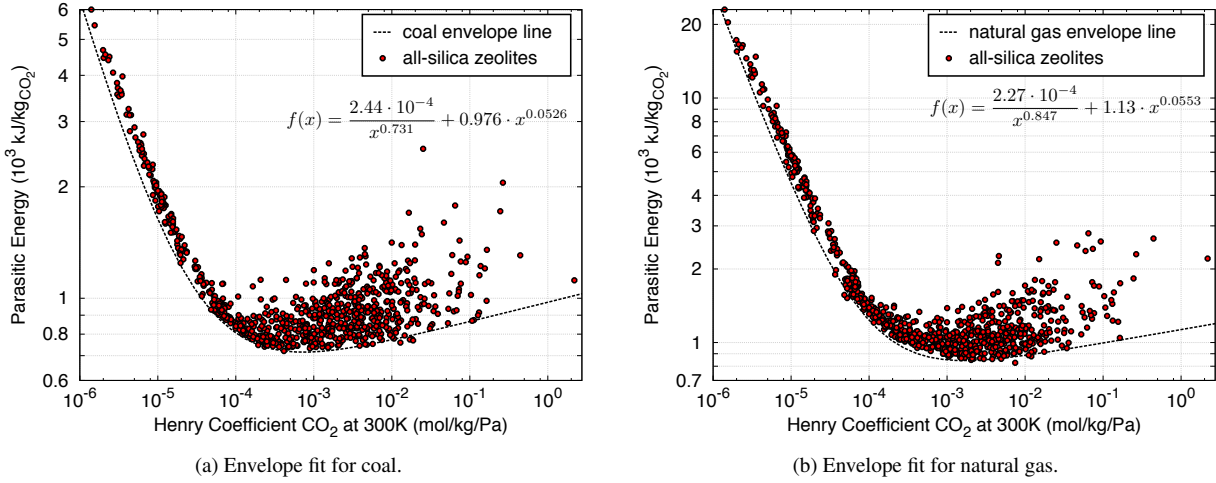


Figure 2: Parasitic energy envelope lines for coal and natural gas of IZA zeolites and predicted structures⁷. Red circles represent the parasitic energies of these all-silica zeolites. Dashed lines indicate the corresponding envelopes. The fitting parameters for the coal case are $a = 2.44 \cdot 10^{-4}$, $n = 0.731$, $b = 0.976$, and $m = 0.0526$. The natural gas fitting parameters were calculated to be $a = 2.27 \cdot 10^{-4}$, $n = 0.847$, $b = 1.13$, and $m = 0.0553$.

4 Heat capacity impact on parasitic energy

Another very important parameter for the parasitic energy calculation is the specific heat capacity C_p of each material. Unfortunately, only a limited number of specific heat capacities has already been measured and reported in literature. An alternative way to get the specific heat capacities is by determine them by quantum calculations. Density functional theory calculations are quite expensive and time-consuming, hence not a preferable option.

Regarding this study a center value ($C_p = 0.985 \text{ J/gK}$), based on a lower and upper bound was used in most cases to compute the parasitic energy. The limits applied on the heat capacity are reported by Mu and Walton in⁸ and correspond to true specific heat capacities values of MOF-5 ($C_p = 0.761 \text{ J/gK}$, lower bound) and LaCu-MOF ($C_p = 1.21 \text{ J/gK}$, upper bound) at 333 K. Additionally, the heat capacity is assumed not to be a strong function of the process temperature and thus is kept constant in this work.

Figure 3 shows the parasitic energy results for coal including the values for the upper, lower, and center heat capacity values. All results based on the center value are depicted as circles. The colors correspond the different classes of materials, respectively. The parasitic energy uncertainty caused by using an upper and lower heat capacity limits are illustrated as error bars. Further, included is the coal envelope line (dashed line) as well as the current state-of-art technology MEA (dotted line). As shown in figure 3 the main impact of the specific heat capacity on the parasitic energy is restricted to materials indicating low henry coefficients of CO_2 ($k_H = 2 \cdot 10^{-6} - 6 \cdot 10^{-5} \text{ mol/kgPa}$). Their ability and preference to adsorb CO_2 is already low, thus the sensible heat term (equation (1) first term in main article), which contains the heat capacity value influences the final parasitic energy result more. Compared materials indicating promising parasitic energies appear to be almost independent from the heat capacity uncertainty. The error bars for the materials within CO_2 henry coefficients of $k_H = 1 \cdot 10^{-4} - 1 \cdot 10^{-1} \text{ mol/kgPa}$ are smaller then the actual symbol, which means that the effect of the desorption heat requirement (equation (1) second term in main article) is dominating the final parasitic energy result and the influence of the sensible heat is nearly negligible.

Although the correct specific heat capacities are not available the results based on the center value provide a sophisticated guess in which parasitic energy region the materials are to be expected.

The strategy of choosing a heat capacity value was necessary, in particular, for hypothetical and not yet synthesized materials. For the heat capacity estimation of the zeolites with exchanged cations a different approach⁹ was applied.

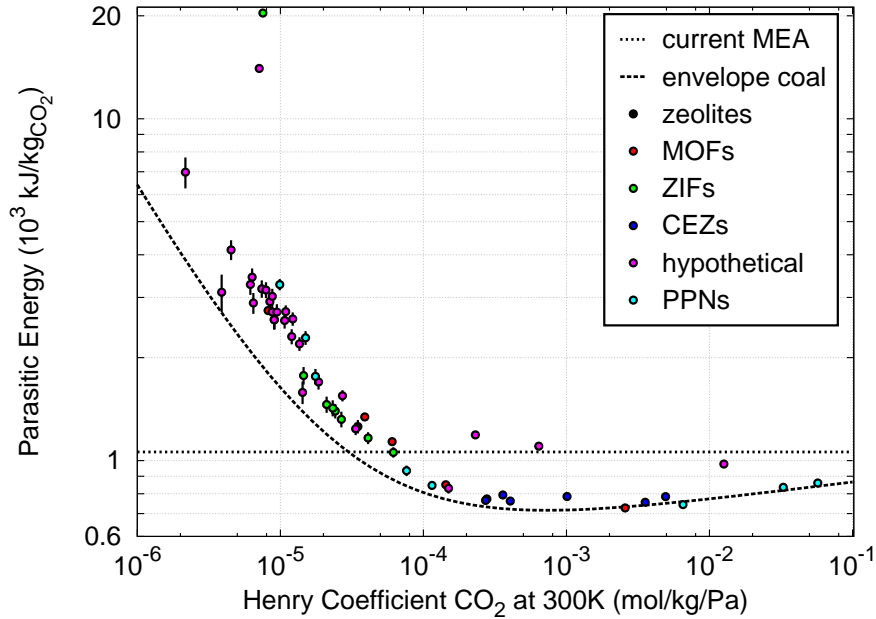


Figure 3: Impact of specific heat capacity on parasitic energy. Circle indicate parasitic energy results using center value as heat capacity. Error bars illustrate the parasitic energy uncertainty by applying the upper and lower limits. Dashed line corresponds to the coal envelope line. As a dotted line the current state-of-art technology of MEA is shown.

5 Energy loss calculation

To estimate the energy loss (EL) caused by applying CCS to power plants the parasitic energy results (PE) needs to be normalized by the total energy that is provided per amount produced CO₂.

Based on the values reported by U.S. Energy Information Administration¹ coal and natural gas produce the following amount of total energy per unit of fuel:

$$\text{coal} = 1,842 \text{ kWh/t} \quad \text{natural gas} = 127 \text{ kWh/Mcf.}$$

Expressed in kJ/kg_{fossil fuel} these values correspond to

$$\text{coal} = 6,631.2 \text{ kJ/kg} \quad \text{natural gas} = 21,023.3 \text{ kJ/kg}$$

(using the conversion factors: 1 cf = 0.02832 m³, 1 kWh = 3.6 · 10⁶ J, and ρ_{natural gas} = 0.768 kg/m³). To normalize the predicted parasitic energies the amount of produced CO₂ per amount consumed fossil fuel needs to be known. These can also be found on the U.S. Energy Information Administration homepage:²

$$\begin{aligned} \text{coal (Sub-bituminous)} &= 2.16 \text{ LbsCO}_2/\text{kWh} = 1.80 \text{ kgCO}_2/\text{kg}_{\text{coal}} \\ \text{natural gas} &= 1.22 \text{ LbsCO}_2/\text{kWh} = 3.23 \text{ kgCO}_2/\text{kg}_{\text{natural gas}} \end{aligned}$$

(conversion factor: 1 Lbs = 0.4536 kg).

The energy loss in case of coal and natural gas is included in table 2 for materials under investigation.

¹U.S. Energy Information Administration, How much coal, natural gas, or petroleum is used to generate a kilowatt-hour of electricity? (eia, Jan. 2014) ; <http://www.eia.gov/tools/faqs/faq.cfm?id=667&t=2>

²U.S. Energy Information Administration, How much carbon dioxide (CO₂) is produced per kilowatthour when generating electricity with fossil fuels? (eia, Jan. 2014) ; <http://www.eia.gov/tools/faqs/faq.cfm?id=74&t=11>

6 Summarized data

Tables 2 & 3 summarize all used and calculated values for all investigated materials. The majority of parasitic energy results are shown as upper, center and lower value, due to the uncertainty of the specific heat capacity. For materials only indicating one parasitic energy value the specific heat capacity was either estimated by quantum calculations or a reported value was found in the literature. All heat of adsorptions, henry coefficients, and saturation loadings are based on $T = 300$ K, parasitic energies are calculated by using IAST.

Table 2: Summarized parameters for all materials. Units: Material density ρ (kg/m³), specific heat capacity C_p (J/kgK), heat of adsorption ΔH (kJ/mol), henry coefficient k_H (mol/kgPa), saturation loading q_{sat} (mol/kg). Parameters ΔH , k_H , and q_{sat} refer to $T = 300$ K.

structure	ρ	C_p	CO ₂				N ₂				
			ΔH_1	$k_{H,1}$	$q_{sat,1}$	ΔH_2	$k_{H,2}$	$q_{sat,2}$	ΔH_1	$k_{H,1}$	$q_{sat,1}$
CaA	1514.0	9851210 ₇₆₁	-58.66	4.93e-03	3.94	-14.53	3.54e-05	1.6	-13.02	6.17e-06	5.54
CaX	1426.0	9851210 ₇₆₁	-41.02	1.01e-03	3.19	-30.65	5.09e-05	3.55	-5.06	4.08e-06	6.74
MgA	1514.0	9851210 ₇₆₁	-36.72	3.59e-04	3.58	-26.5	8.89e-06	1.57	-24.73	2.89e-06	5.15
MgX	1426.0	9851210 ₇₆₁	-40.85	4.05e-04	3.38	-32.58	3.82e-05	3.3	-24.93	2.05e-06	6.69
NaA	1514.0	9851210 ₇₆₁	-30.12	2.72e-04	2.4	-30.09	1.71e-05	1.57	-8.34	8.86e-07	3.97
NaX	1426.0	9851210 ₇₆₁	-50.11	3.55e-03	2.5	-37.4	1.77e-04	3.81	-15.11	3.55e-06	6.31
PS-MFI	1838.0	8631210 ₇₆₁	-26.23	3.48e-05	3.44				-22.26	1.77e-06	3.439
Mg-MOF-74	914.88	896	-37.36	2.57e-03	6.32	-19.81	2.77e-05	9.08	-18.73	1.1e-05	5.0
Zn-MOF-74	1219.39	684	-25.02	1.43e-04	10.21				-13.45	3.01e-06	10.18
Co-MOF-74	1180.54	9851210 ₇₆₁	-36.54	3.0e-04	8.66				-12.4	6.64e-06	8.66
Ni-MOF-74	1194.09	9851210 ₇₆₁	-45.87	4.71e-04	2.41	-20.69	7.92e-05	6.59	-25.32	1.25e-05	6.65
MOF-177	426.74	840	-13.71	8.21e-06	25.0				-10.89	1.83e-06	5.0
CuBTC	948.8	1158	-27.49	6.05e-05	17.58				-15.35	2.62e-06	5.63
CuBTTri	789.0	9851210 ₇₆₁	-24.26	3.89e-05	42.6				-1.92	2.37e-06	5.0
mmen-CuBTTri	1059.0	9851210 ₇₆₁	-53.0	2.78e-04	4.68				-24.55	1.24e-06	0.3
UMCM-1	429.0	851.3	-10.92	9.87e-06	150.0				-5.45	1.75e-06	55.0
SIFSIX-3-Cu	1728.0	985	-47.52	3.14e-02	2.4	-3.76	2.09e-06	0.4	-10.81	1.93e-06	2.8
SIFSIX-3-Zn	1574.0	985	-41.5	3.47e-03	2.6	-27.87	1.32e-06	0.286	-12.21	2.91e-06	2.886
ZIF-8	949.0	9851210 ₇₆₁	-20.96	7.55e-06	14.2				-13.2	2.33e-05	122.2
ZIF-68	900.77	9851210 ₇₆₁	-23.99	2.11e-05	5.836				-15.44	1.18e-06	4.291
ZIF-69	998.74	9851210 ₇₆₁	-22.21	2.42e-05	6.237				-13.2	1.37e-06	5.948
ZIF-70	747.24	9851210 ₇₆₁	-19.88	1.45e-05	8.477				-14.28	1.30e-06	1.728
ZIF-78	1023.9	9851210 ₇₆₁	-26.63	6.17e-05	3.569				-13.3	1.80e-06	3.367
ZIF-79	937.03	9851210 ₇₆₁	-25.98	2.33e-05	3.564				-14.85	1.18e-06	1.883
ZIF-81	1124.27	9851210 ₇₆₁	-25.52	2.67e-05	3.878				-14.23	1.19e-06	2.173
ZIF-82	815.86	9851210 ₇₆₁	-24.92	4.10e-05	4.944				-13.79	1.52e-06	3.414
PPN-4	284.1	9851210 ₇₆₁	-13.86	9.9e-06	120.0				-6.61	3.02e-06	8.2
PPN-6	325.0	9851210 ₇₆₁	-16.35	1.5e-05	12.0				-7.31	2.9e-06	0.5
PPN-6-CH ₂ Cl	528.0	9851210 ₇₆₁	-20.05	1.76e-05	10.4				-8.56	1.76e-06	0.63
PPN-6-SO ₃ H	642.0	9851210 ₇₆₁	-27.82	7.62e-05	6.0				-9.27	2.32e-06	0.4
PPN-6-SO ₃ Li	666.0	9851210 ₇₆₁	-30.27	1.15e-04	5.0				-7.13	2.6e-06	0.4
PPN-6-CH ₂ DETA	805.0	9851210 ₇₆₁	-45.33	5.71e-02	5.35				-17.99	7.65e-07	0.1
PPN-6-CH ₂ TAEA	982.5	9851210 ₇₆₁	-35.01	3.28e-02	4.82				-14.91	9.38e-07	0.02
PPN-6-CH ₂ TETA	883.8	9851210 ₇₆₁	-48.23	6.52e-03	4.77				-18.29	6.99e-07	0.04
ZIF-36-CAG	2006.5	9851210 ₇₆₁	-51.77	1.26e-02	1.48				-25.38	6.48e-06	1.48
ZIF-36-FRL	1808.87	9851210 ₇₆₁	-40.66	1.50e-04	2.01	-24.39	2.15e-06	1.01	-18.75	4.74e-07	3.02
ZIF-39-DIA	1009.17	9851210 ₇₆₁	-28.88	1.43e-05	10.35				-16.34	5.4e-07	10.35
ZIF-39-ZNI	1497.35	9851210 ₇₆₁	-30.47	2.17e-06	1.29				-22.36	9.74e-07	1.29
ZIF-40-GIS	1254.51	9851210 ₇₆₁	-33.26	2.31e-04	2.21	-3.66	5.38e-06	3.76	-22.14	1.03e-05	5.97
ZIF-116-CAG	1353.83	9851210 ₇₆₁	-37.81	6.41e-04	2.14	-20.79	2.06e-06	2.51	-24.35	1.53e-05	4.65
ZIF-116-MER	850.95	9851210 ₇₆₁	-22.04	2.72e-05	16.57				-11.51	2.38e-06	16.57
ZIF-116-SOD	855.31	9851210 ₇₆₁	-17.95	1.2e-05	14.15				-11.27	2.01e-06	14.15
HMOF-MOF-5	572.98	9851210 ₇₆₁	-14.96	8.45e-06	27.37				-8.01	1.97e-06	27.37
HMOF-16	701.06	9851210 ₇₆₁	-22.68	3.36e-05	30.47				-8.37	1.61e-06	1.54
HMOF-27	777.34	9851210 ₇₆₁	-12.53	4.52e-06	52.91				-8.42	1.7e-06	1.48
HMOF-96	576.92	9851210 ₇₆₁	-14.49	7.12e-06	138.61				-8.59	2.26e-05	1.71
HMOF-163	1000.38	9851210 ₇₆₁	-17.63	8.77e-06	15.07				-11.68	1.93e-06	1.02

HMOF-469	873.26	985 ¹²¹⁰ ₇₆₁	-15.56	6.47e-06	34.32		-8.37	1.25e-06	14.79
HMOF-541	905.88	985 ¹²¹⁰ ₇₆₁	-17.99	9.05e-06	20.5		-10.91	1.75e-06	0.96
HMOF-602	905.88	985 ¹²¹⁰ ₇₆₁	-17.99	9.07e-06	19.75		-10.91	1.75e-06	1.03
HMOF-611	648.95	985 ¹²¹⁰ ₇₆₁	-17.11	9.46e-06	51.07		-9.36	2.05e-06	1.68
HMOF-646	245.77	985 ¹²¹⁰ ₇₆₁	-12.59	7.95e-06	81.57		-5.49	2.64e-06	81.57
HMOF-785	639.42	985 ¹²¹⁰ ₇₆₁	-15.24	8.78e-06	43.51		-9.47	2.42e-06	1.66
HMOF-972	670.41	985 ¹²¹⁰ ₇₆₁	-14.75	6.35e-06	58.92		-9.29	1.91e-06	1.58
HMOF-992	624.98	985 ¹²¹⁰ ₇₆₁	-21.31	1.85e-05	24.41		-8.35	1.55e-06	24.41
HMOF-1041	409.13	985 ¹²¹⁰ ₇₆₁	-14.65	1.09e-05	41.81		-7.45	2.44e-06	41.81
HMOF-1055	711.3	985 ¹²¹⁰ ₇₆₁	-16.03	1.22e-05	27.59		-10.51	2.94e-06	1.58
HMOF-1631	834.9	985 ¹²¹⁰ ₇₆₁	-17.15	1.07e-05	27.62		-10.91	2.35e-06	1.12
HMOF-1708	765.19	985 ¹²¹⁰ ₇₆₁	-15.39	7.42e-06	32.57		-10.0	2.1e-06	1.37
HMOF-1927	849.84	985 ¹²¹⁰ ₇₆₁	-14.77	6.17e-06	32.86		-9.57	1.67e-06	1.09
HMOF-1996	612.16	985 ¹²¹⁰ ₇₆₁	-14.67	7.94e-06	61.59		-8.94	2.26e-06	1.71
HMOF-2368	226.63	985 ¹²¹⁰ ₇₆₁	-12.17	7.65e-06	100.01		-5.27	2.78e-06	100.01

The parameters presented in tab. 2 are based on the following experimental references: MOFs^{3,10–21}, PPNs^{22,23}, ZIFs^{24–26}, CEZs². Properties of hypothetical materials were predicted by GCMC simulations.

Table 3: Summarized results for all gas compositions & regeneration strategies. Units: Parasitic energies PE_{comp} (MJ/kgCO₂), and energy loss EL_{comp} (%). Heating energy and compression work for PSA & TSA are also shown in (MJ/kgCO₂), respectively. All shown PE results are based on IAST.

structure	PE _{coal}	EL _{coal}	PE NG	EL _{NG}	PE _{air}	PSA		TSA	
						heating	compression	heating	compression
CaA	0.784 ^{0.794} _{0.774}	21.3	0.943	14.5	3.6	0.208	0.576	0.557	0.37
CaX	0.785 ^{0.796} _{0.774}	21.3	1.06	16.3	17.6	0.167	0.618	0.595	0.395
MgA	0.793 ^{0.807} _{0.778}	21.5	1.17	18	62	0.178	0.615	0.77	0.408
MgX	0.76 ^{0.774} _{0.749}	20.6	1.06	16.3	36.8	0.186	0.574	0.625	0.39
NaA	0.765 ^{0.783} _{0.745}	20.8	1.05	16.1	85.6	0.177	0.588	1.19	0.382
NaX	0.754 ^{0.767} _{0.744}	20.5	0.925	14.2	4.57	0.191	0.563	0.528	0.371
PS-MFI	1.23 ^{1.31} _{1.2}	33.3	2.9	44.6	1.11e+03	0.322	0.904	4.62	0.615
Mg-MOF-74	0.727	19.7	0.959	14.7	16	0.142	0.585	0.463	0.378
Zn-MOF-74	0.85	23.1	1.56	23.9	250	0.134	0.716	1.11	0.47
Co-MOF-74	0.90 ^{0.918} _{0.896}	24.6	1.71	26.3	91.7	0.168	0.739	0.659	0.494
Ni-MOF-74	0.96 ^{0.97} _{0.95}	26.1	1.74	26.8	110	0.182	0.778	0.943	0.5
MOF-177	2.75	74.6	9.79	150	6.04e+04	0.659	2.09	82.8	2
CuBTC	1.14	30.8	2.65	40.7	723	0.265	0.872	3.07	0.599
CuBTTri	1.34 ^{1.39} _{1.3}	36.4	3.58	55	1.33e+03	0.27	1.07	4.81	0.781
mnen-CuBTTri	0.752 ^{0.788} _{0.757}	20.4	1.11	17	30	0.248	0.505	0.574	0.363
UMCM-1	2.38	64.7	8.24	127	2.81e+05	0.515	1.87	111	1.84
SIFSIX-3-Cu	0.94	25.5	0.963	14.8	1.62	0.211	0.729	1.4	0.357
SIFSIX-3-Zn	0.805	21.8	0.907	13.9	5.81	0.201	0.604	0.881	0.364
ZIF-8	20.4 ^{20.6} _{20.2}	553	89.8	1.38e+03	2.89e+04	1.89	18.5	46.9	16.4
ZIF-68	1.46 ^{1.54} _{1.38}	39.6	3.85	59.2	2.64e+03	0.438	1.02	9.64	0.714
ZIF-69	1.4 ^{1.46} _{1.33}	37.9	3.63	55.8	2.76e+03	0.381	1.01	9.35	0.719
ZIF-70	1.77 ^{1.88} _{1.67}	48.1	5.28	81.1	7.89e+03	0.557	1.22	20.7	0.925
ZIF-78	1.06 ^{1.09} _{1.02}	28.7	2.22	34.1	653	0.25	0.807	3.22	0.538
ZIF-79	1.42 ^{1.5} _{1.34}	38.7	3.68	56.5	1.96e+03	0.433	0.992	8.09	0.708
ZIF-81	1.32 ^{1.39} _{1.25}	35.8	3.26	50.1	1.69e+03	0.4	0.92	7.06	0.624
ZIF-82	1.16 ^{1.21} _{1.12}	31.6	2.68	41.2	1.18e+03	0.289	0.875	4.85	0.594
PPN-4	3.27 ^{3.4} _{3.15}	88.8	12.3	188	6.43e+04	0.627	2.64	85.1	2.67

PPN-6	2.29 ^{2.39} _{2.18}	62	8.2	126	3e+04	0.53	1.76	46.7	1.55
PPN-6-CH ₂ Cl	1.76 ^{1.85} _{1.67}	47.9	5.48	84.2	7.98e+03	0.491	1.27	19.6	0.976
PPN-6-SO ₃ H	0.934 ^{0.966} _{0.901}	25.4	2.07	31.8	638	0.23	0.704	2.64	0.454
PPN-6-SO ₃ Li	0.846 ^{0.871} _{0.82}	23	1.7	26.2	338	0.202	0.644	1.69	0.419
PPN-6-CH ₂ DETA	0.86 ^{0.876} _{0.843}	23.3	0.88	13.5	1.21	0.21	0.65	0.815	0.356
PPN-6-CH ₂ TAEA	0.835 ^{0.885} _{0.816}	22.7	0.858	13.2	1.65	0.187	0.648	1.2	0.356
PPN-6-CH ₂ TETA	0.742 ^{0.756} _{0.731}	20.2	0.807	12.4	1.95	0.209	0.534	0.511	0.358
ZIF-36-CAG	0.977 ^{0.997} _{0.949}	26.5	1.02	15.7	3.24	0.242	0.735	1.48	0.361
ZIF-36-FRL	0.829 ^{0.858} _{0.8}	22.5	1.21	18.6	72.6	0.253	0.576	1.18	0.384
ZIF-39-DIA	1.58 ^{1.7} _{1.46}	43	4.2	64.6	2.26e+03	0.623	0.96	10.5	0.661
ZIF-39-ZNI	6.98 ^{7.7} _{6.23}	189	26.3	404	4.58e+04	3.57	3.41	143	4.22
ZIF-40-GIS	1.19 ^{1.21} _{1.17}	32.3	2.5	38.4	418	0.208	0.981	2.57	0.706
ZIF-116-CAG	1.1 ^{1.12} _{1.09}	29.9	1.93	29.6	124	0.199	0.903	1.17	0.542
ZIF-116-MER	1.55 ^{1.61} _{1.49}	42	4.38	67.3	2.59e+03	0.346	1.2	8.17	0.901
ZIF-116-SOD	2.3 ^{2.42} _{2.19}	62.6	7.63	117	1.25e+04	0.604	1.7	29.2	1.38
HMOF-MOF-5	2.92 ^{3.07} _{2.77}	79.2	10.4	160	4.18e+04	0.753	2.16	69.2	2.04
HMOF-16	1.24 ^{1.29} _{1.19}	33.6	3.14	48.3	1.98e+03	0.303	0.936	6.55	0.65
HMOF-27	4.13 ^{4.41} _{3.85}	112	15.9	244	2.11e+05	1.33	2.8	226	2.9
HMOF-96	14 ^{14.3} _{13.8}	381	63.6	978	1.69e+05	1.43	12.6	184	13.1
HMOF-163	2.72 ^{2.89} _{2.56}	73.9	9.58	147	2.26e+04	0.834	1.89	47.1	1.64
HMOF-469	2.89 ^{3.09} _{2.69}	78.4	10.1	155	4.4e+04	0.966	1.92	79.5	1.7
HMOF-541	2.58 ^{2.74} _{2.42}	70.1	8.95	138	2.08e+04	0.802	1.78	44.1	1.49
HMOF-602	2.58 ^{2.74} _{2.42}	70.1	8.94	137	2.05e+04	0.798	1.78	43.7	1.49
HMOF-611	2.72 ^{2.87} _{2.57}	73.8	9.6	148	2.47e+04	0.738	1.98	47.9	1.77
HMOF-646	3.62 ^{3.77} _{3.48}	98.3	13.8	212	2.09e+05	0.711	2.91	146	3.12
HMOF-785	3.02 ^{3.18} _{2.87}	82.1	11.1	170	4.13e+04	0.779	2.25	67.8	2.06
HMOF-972	3.44 ^{3.65} _{3.23}	93.4	12.8	197	7.05e+04	1.01	2.43	106	2.33
HMOF-992	1.7 ^{1.78} _{1.61}	46.1	4.98	76.5	4.57e+03	0.443	1.25	13.5	0.946
HMOF-1041	2.73 ^{2.84} _{2.61}	74	9.68	149	3.62e+04	0.592	2.14	57.3	2
HMOF-1055	2.6 ^{2.71} _{2.48}	70.5	9.22	142	2.24e+04	0.61	1.99	41.1	1.74
HMOF-1631	2.57 ^{2.71} _{2.43}	69.8	9.03	139	2.05e+04	0.695	1.87	41	1.56
HMOF-1708	3.18 ^{3.37} ₃	86.4	11.7	180	4.74e+04	0.913	2.27	78.7	2.12
HMOF-1927	3.27 ^{3.49} _{3.05}	88.9	12	185	6.73e+04	1.06	2.22	105	2.05
HMOF-1996	3.15 ^{3.32} _{2.99}	85.6	11.6	179	5.45e+04	0.833	2.32	83.5	2.23
HMOF-2368	3.82 ^{3.97} _{3.68}	104	14.8	227	7.6e+05	0.722	3.1	171	3.37

References

- [1] A. L. Dzubak, L.-C. Lin, J. Kim, J. A. Swisher, R. Poloni, S. N. Maximoff, B. Smit and L. Gagliardi, *Nature Chemistry*, 2012, **4**, 810–816.
- [2] T.-H. Bae, M. R. Hudson, J. A. Mason, W. L. Queen, J. J. Dutton, K. Sumida, K. J. Micklash, S. S. Kaye, C. M. Brown and J. R. Long, *Energy & Environmental Science*, 2013, **6**, 128.
- [3] T. M. McDonald, D. M. D'Alessandro, R. Krishna and J. R. Long, *Chemical Science*, 2011, **2**, 2022.
- [4] *Direct Air Capture of CO₂ with Chemicals*, 2011, <http://www.aps.org/policy/reports/assessments/upload/dac2011.pdf>.
- [5] A. S. Bhowm and B. C. Freeman, *Environmental science & technology*, 2011, **45**, 8624–32.
- [6] B. Smit, J. R. Reimer, C. M. Oldenburg and I. C. I. C. Bourg, *Introduction to Carbon Capture and Sequestration*, Imperial College Press, London, 1st edn., 2014.
- [7] L.-C. Lin, A. H. Berger, R. L. Martin, J. Kim, J. A. Swisher, K. Jariwala, C. H. Rycroft, A. S. Bhowm, M. W. Deem, M. Haranczyk and B. Smit, *Nature materials*, 2012, **11**, 633–41.
- [8] B. Mu and K. S. Walton, *The Journal of Physical Chemistry C*, 2011, **115**, 22748–22754.
- [9] P. Vieillard, *European Journal of Mineralogy*, 2010, **22**, 823–836.
- [10] P. Aprea, D. Caputo, N. Gargiulo, F. Iucolano and F. Pepe, *Journal of Chemical & Engineering Data*, 2010, **55**, 3655–3661.
- [11] P. Chowdhury, S. Mekala, F. Dreisbach and S. Gumma, *Microporous and Mesoporous Materials*, 2012, **152**, 246–252.
- [12] P. D. C. Dietzel, V. Besikiotis and R. Blom, *Journal of Materials Chemistry*, 2009, **19**, 7362.
- [13] P. D. C. Dietzel, R. Blom and H. Fjellvåg, *European Journal of Inorganic Chemistry*, 2008, **2008**, 3624–3632.
- [14] L. Grajciar, A. D. Wiersum, P. L. Llewellyn, J.-S. Chang and P. Nachtigall, *The Journal of Physical Chemistry C*, 2011, **115**, 17925–17933.
- [15] Z. Liang, M. Marshall and A. L. Chaffee, *Energy & Fuels*, 2009, **23**, 2785–2789.
- [16] J. A. Mason, K. Sumida, Z. R. Herm, R. Krishna and J. R. Long, *Energy & Environmental Science*, 2011, **4**, 3030.
- [17] B. Mu, P. M. Schoenecker and K. S. Walton, *The Journal of Physical Chemistry C*, 2010, **114**, 6464–6471.
- [18] J. M. Simmons, H. Wu, W. Zhou and T. Yildirim, *Energy & Environmental Science*, 2011, **4**, 2177.
- [19] K. Uemura, A. Maeda, T. K. Maji, P. Kanoo and H. Kita, *European Journal of Inorganic Chemistry*, 2009, **2009**, 2329–2337.
- [20] P. Nugent, Y. Belmabkhout, S. D. Burd, A. J. Cairns, R. Luebke, K. Forrest, T. Pham, S. Ma, B. Space, L. Wojtas, M. Eddaoudi and M. J. Zaworotko, *Nature*, 2013, **495**, 80–4.
- [21] O. Shekhah, Y. Belmabkhout, Z. Chen, V. Guillerm, A. Cairns, K. Adil and M. Eddaoudi, *Nature communications*, 2014, **5**, 4228.
- [22] W. Lu, J. P. Sculley, D. Yuan, R. Krishna, Z. Wei and H.-C. Zhou, *Angewandte Chemie (International ed. in English)*, 2012, **51**, 7480–4.
- [23] W. Lu, D. Yuan, J. Sculley, D. Zhao, R. Krishna and H.-C. Zhou, *Journal of the American Chemical Society*, 2011, **133**, 18126–9.
- [24] H. Amrouche, S. Aguado, J. Pérez-Pellitero, C. Chizallet, F. Siperstein, D. Farrusseng, N. Bats and C. Nieto-Draghi, *The Journal of Physical Chemistry C*, 2011, **115**, 16425–16432.

- [25] R. Banerjee, H. Furukawa, D. Britt, C. Knobler, M. O'Keeffe and O. M. Yaghi, *Journal of the American Chemical Society*, 2009, **131**, 3875–7.
- [26] H. Huang, W. Zhang, D. Liu, B. Liu, G. Chen and C. Zhong, *Chemical Engineering Science*, 2011, **66**, 6297–6305.